

UniDA3D: Unified Domain Adaptive 3D Semantic Segmentation Pipeline

Ben Fei^{*,1}, Siyuan Huang³, Jiakang Yuan¹, Botian Shi²,
Bo Zhang^{†,2}, Weidong Yang^{†,1}, Min Dou², Yikang Li²

¹Fudan University ²Shanghai AI Laboratory, ³Shanghai Jiaotong University

bfei21@m.fudan.edu.cn, siyuan.sjtu@sjtu.edu.cn, jkyuan22@m.fudan.edu.cn

Abstract

State-of-the-art 3D semantic segmentation models are trained on off-the-shelf public benchmarks, but they will inevitably face the challenge of recognition accuracy drop when these well-trained models are deployed to a new domain. In this paper, we introduce a Unified Domain Adaptive 3D semantic segmentation pipeline (UniDA3D) to enhance the weak generalization ability, and bridge the point distribution gap between domains. Different from previous studies that only focus on a single adaptation task, UniDA3D can tackle several adaptation tasks in 3D segmentation field, by designing a unified source-and-target active sampling strategy, which selects a maximally-informative subset from both source and target domains for effective model adaptation. Besides, benefiting from the rise of multi-modal 2D-3D datasets, UniDA3D investigates the possibility of achieving a multi-modal sampling strategy, by developing a cross-modality feature interaction module that can extract a representative pair of image and point features to achieve a bi-directional image-point feature interaction for safe model adaptation. Experimentally, UniDA3D is verified to be effective in many adaptation tasks including: 1) unsupervised domain adaptation, 2) unsupervised few-shot domain adaptation; 3) active domain adaptation. Their results demonstrate that, by easily coupling UniDA3D with off-the-shelf 3D segmentation baselines, domain generalization ability of these baselines can be enhanced.

1. Introduction

In recent years, 3D semantic segmentation models[11, 36, 14] have achieved remarkable gains, owing to the large-scale annotated datasets, such as SemanticKITTI [1] and nuScenes [3], etc. However, 3D semantic segmentation

*This work was done when Ben Fei was an intern at Shanghai AI Laboratory.

†Corresponding to: Bo Zhang (zhangbo@pjlab.org.cn), Weidong Yang (wdyang@fudan.edu.cn)

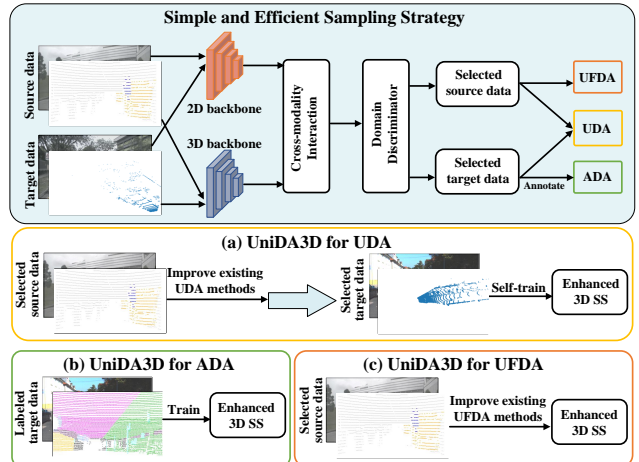


Figure 1. Our UniDA3D leverages a **unified** multi-modal sampling strategy that can effectively address various DA tasks: (a) UDA, (b) ADA, and (c) UFDA.

models still suffer from a severe performance drop issue when they are directly deployed to a novel domain. Actually, one straightforward method to alleviate such a performance drop issue is to build a specific dataset for the novel domain, by extensively collecting target-domain data and performing labor-intensive human annotation [30, 8]. But this is impractical in many real-world applications such as autonomous driving.

Domain Adaptation (DA), as one of the typical techniques in the transfer learning community, aims to tackle the above-mentioned performance drop issue by learning domain-invariant representations [40, 33, 23], which includes Unsupervised Domain Adaptation (UDA), Unsupervised Few-shot Domain Adaptation (UFDA), and Active Domain Adaptation (ADA) tasks, according to the condition of the target domain. Recently, inspired by UDA in 2D image [46, 2, 39], some researchers [16, 25, 20] try to address the 3D point cloud-induced domain variations under a **single adaptation task** such as the UDA setting. For example, xMUDA [16] attempts to extract 2D and 3D features using two different network branches, exploiting the inter-modal feature complementarity. However, different from

these UDA 3D segmentation works that focus on leveraging multi-modal data only under **a single adaptation task** (*i.e.* UDA), we aim to develop a unified domain adaptive segmentation method for achieving a safe-and-unified 3D segmentation model transfer under **several adaptation tasks**.

To design a unified method that can be effective under different DA task settings, we resort to exploring a model-agnostic or task-agnostic strategy. We observe that, during the 3D model source-to-target adaptation process, there are many irrelevant source-domain samples and redundant target-domain samples. On the one hand, due to the intra-domain feature variations, some samples from the source domain may present a large data distribution difference from the target domain data. Learning from such irrelevant source-domain samples will be harmful to the model transfer towards the target domain, since the source-only model will fit the feature distribution that is quite different from the target domain, causing an irrelevant source-domain adaptation. On the other hand, in autonomous driving scenarios, samples within the same target-domain sequence have a similar data distribution, which results in redundant target-domain adaptation by self-training UDA methods [47, 22, 45]. Thus, we propose a Unified Domain Adaptive 3D semantic segmentation (UniDA3D) pipeline, which can pick up a maximally-informative subset from both source and target domains to reduce the difficulty of model source-to-target adaptation.

Besides, our UniDA3D also can fully leverage the multi-modal data from different domains to perform a multi-modal balanced sampling process. During the model adaptation process, UniDA3D uses a cross-modality feature interaction module, which encodes features from a single image or point cloud modality, and then performs an image-to-point and point-to-image feature-level information interaction by a symmetrical cross-branch attention structure. Furthermore, the learned cross-modal features (Fig. 3) are utilized as an important proxy for the subsequent sampling process, which is versatile to many DA tasks. As illustrated in Fig. 1, such a subset sampling way can be easily combined with the off-the-shelf DA variants, achieving a better source-domain pre-trained performance and a promising target-domain adaptation performance.

The main contributions can be summarized as follows:

1. We explore the possibilities of leveraging bi-domain cross-modal sampling method to achieve a unified domain adaptive 3D semantic segmentation.
2. UniDA3D pipeline is proposed, which utilizes a cross-modality feature interaction module to fuse the feature’s multi-modal information, boosting the model’s adaptation performance.
3. UniDA3D can be deployed to many adaptation tasks simultaneously, which include: 1) UDA task where all data from the target domain are unlabeled; 2)

UFDA task where we can only access few-shot unlabeled samples from the target domain; 3) ADA task where a portion of unlabeled target data is selected to be annotated by an oracle. Experiments are conducted on several public benchmarks, including nuScenes [3], A2D2 [10], SemanticKITTI [1], and VirtualKITTI [17], and their results show that UniDA3D can be easily applied to multiple adaptation tasks, to enhance the model transferability, outperforming the existing works, xMUDA [16], AUDA [20], and DsCML [25] by 7.75%, 7.92%, and 4.61%.

2. Related Works

2.1. Active Domain Adaptation

Active learning aims to develop annotation-efficient algorithms via sampling the most representative samples to be labeled by an oracle [28]. Most recently, active learning coupled with domain adaptation, termed as Active Domain Adaptation (ADA), has great practical significance. Nevertheless, only a few previous researchers focus on addressing the problem, pioneered by active adaptation in the area of sentiment classification for text data [27]. Rita et al. [4] choose target samples to learn importance weights for source instances by solving a convex optimization problem of minimizing Maximum Mean Discrepancy (MMD). Recently, Su et al. [31] try to study ADA problem in the context of Convolution Neural Networks (CNN), and instances are selected based on their designed uncertainty and “targetness”. However, these sampling strategies are designed based on the 2D image domain, and it is intractable to directly apply these 2D image-based sampling strategies to the 3D image-point multi-modal task. In our work, for the first time, we design a novel active-and-adaptive segmentation baseline to sample the most informative 2D-3D pairs to enhance the weak cross-domain generalization ability of a well-trained 3D segmentation model.

2.2. General and UDA 3D Semantic Segmentation

In 3D semantic segmentation, 3D point clouds are often represented as voxels. For instance, SSCNs [11] and the following works [7, 15, 41] leverage hash tables to convolve only on sampled voxels, allowing for very high resolution with typically only one point per voxel. Point-based methods conduct computation in continuous 3D space and can directly take point clouds as input. PointNet++ [26] utilizes point-wise convolution and max-pooling to extract global features and local neighborhood aggregation for hierarchical learning with CNN. Following that, continuous convolutions [37] and deformable kernels [32] have been proposed. DGCNN [38] and LDGCNN [44] perform convolution on the edges of a point cloud. More recently, xMUDA [16], AUDA [20], and DsCML [25] utilize point clouds and im-

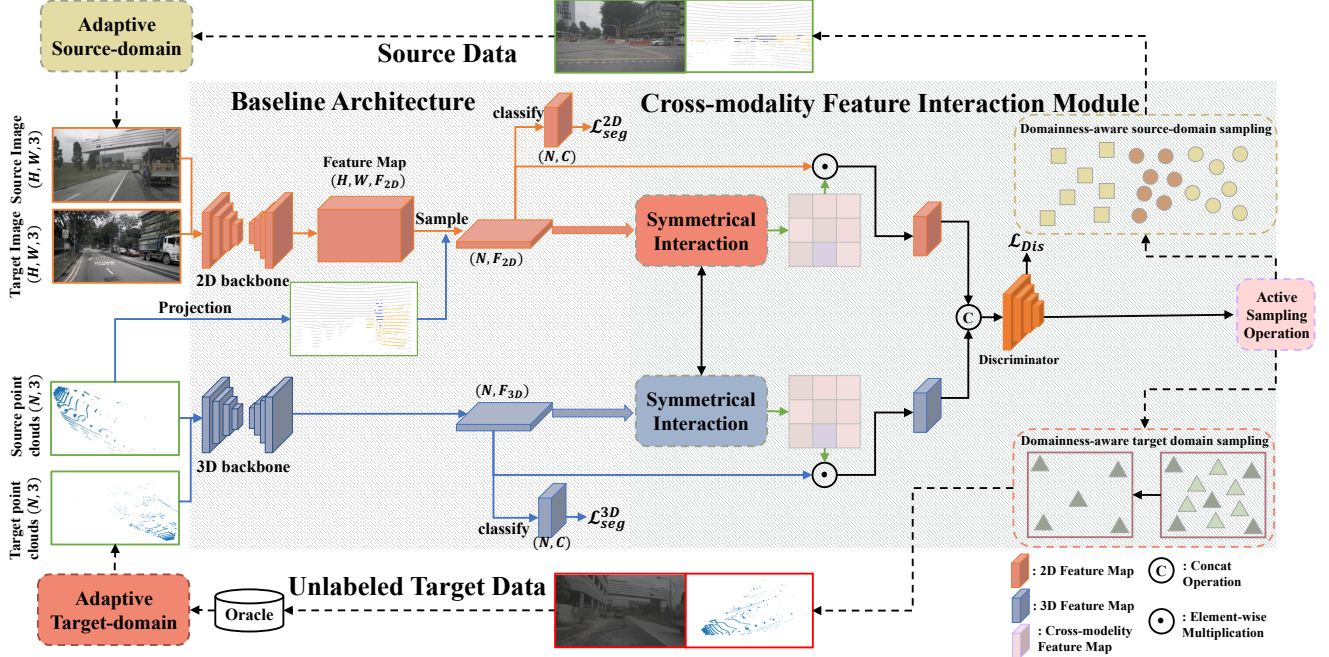


Figure 2. The network architecture of UniDA3D, which consists of a 3D segmentation baseline, the cross-modality feature interaction module, and the active sampling operation. The 3D segmentation baseline comprises a 2D U-Net-Style ConvNet [12] backbone, which takes an image as input, and a 3D U-Net-Style SparseConvNet [11] backbone, which receives a point cloud as input. Cross-modality feature interaction module can leverage the features (F_{2D} and F_{3D}) to exploit a representative pair of image features and point cloud features to achieve a bi-directional image-point feature interaction. The last active sampling operation utilizes the interactive features to perform both the source-domain sampling and target-domain sampling via the unified module.

ages for UDA task in 3D semantic segmentation. However, these methods only focus on UDA task and overlook the intrinsic characteristics of the source and target domain. Therefore, in this work, we try to solve multiple adaptation tasks in a unified pipeline rather than a single adaptation task in 3D semantic segmentation [16, 20, 25].

3. The Proposed Method

Our method is proposed to enhance the adaptability of a 3D semantic segmentation model by assuming the presence of 2D images and 3D point clouds. In this section, we will first define the problem and illustrate the network architecture in Sec. 3.1. Following that, the UniDA3D pipeline is described in Sec. 3.2.

3.1. Preliminary

Problem Definition. Suppose that \mathcal{S} and \mathcal{T} define a source domain and a target domain, both of which contain different modalities including 2D images and 3D point clouds $\{(x_{2D}^s, x_{3D}^s)\}_{i=1}^{n_s}$ and $\{(x_{2D}^t, x_{3D}^t)\}_{i=1}^{n_t}$. The purpose of cross-domain 3D semantic segmentation is to adapt a well-trained segmentation baseline from a labeled source domain \mathcal{S} to a new target domain \mathcal{T} with the data distribution shift.

To design a unified cross-domain 3D semantic segmentation pipeline under different target-domain conditions, we

consider the following adaptation tasks: 1) Unsupervised Domain Adaptation (UDA), where we can access all unlabeled 2D-3D sample pairs from the target domain \mathcal{T} ; 2) Unsupervised Few-shot Domain Adaptation (UFDA), where only a few data (e.g., 5% target data) from the unlabeled target domain \mathcal{T} are available; 3) Active Domain Adaptation (ADA), where one can sample a subset from the full set of the unlabeled target domain and perform the manual annotation process. An annotation budget B_t denotes the total amount of sampled target domain data for ADA task, while a budget B_s is denoted as the total number of sampled source domain data.

3D Segmentation Architecture. Given annotations from the source domain, a segmentation baseline is trained in a supervised manner with cross-entropy loss function for the 2D image x_{2D}^s and 3D point cloud x_{3D}^s as follows:

$$\begin{aligned}\mathcal{L}_{2D}^{seg}(x_{2D}^s, \phi(y_{3D}^s)) &= -\frac{1}{N} \sum_{n=1}^N \sum_{c=1}^C \phi(y_{(n,c)}^s) \log P_{2D}^{(n,c)}, \\ \mathcal{L}_{3D}^{seg}(x_{3D}^s, y_{3D}^s) &= -\frac{1}{N} \sum_{n=1}^N \sum_{c=1}^C y_{(n,c)}^s \log P_{3D}^{(n,c)},\end{aligned}\quad (1)$$

where $y_{(n,c)}^s$ and $P^{(n,c)}$ stand for the ground-truth label and prediction of the point n for the class c , respectively. ϕ is the projection of the point cloud to the front view. Herein, the

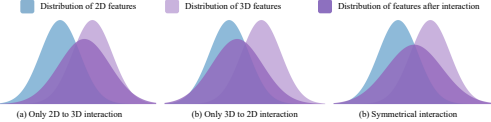


Figure 3. Illustration of unidirectional and symmetrical interaction. (a) The high-level features (f_{2D}, f_{3D}) undergo 2D to 3D interaction will obtain $(\hat{f}_{2D}, \hat{f}_{3D})$, which samples data pairs largely by 3D features; (b) Otherwise, the high-level features (f_{2D}, f_{3D}) go through 3D to 2D interaction will get $(\hat{f}_{2D}, \hat{f}_{3D})$ to sample data pairs taking 2D features into more consideration. (c) To this end, our symmetrical interaction provides a novel way to sample data pairs by considering both 2D and 3D features, leading to a more powerful sampling capability.

overall objective of the source domain can be formulated as:

$$\min_{\theta_{2D}, \theta_{3D}} \frac{1}{N^s} \sum_{x_s \in S} \mathcal{L}_{2D}^{seg}(x_{2D}^s, \phi(y_{3D}^s)) + \mathcal{L}_{3D}^{seg}(x_{3D}^s, y_{3D}^s), \quad (2)$$

where θ_{2D} and θ_{3D} are the parameters of the 2D sub-network and the 3D sub-network, respectively.

3.2. UniDA3D: Unified Domain Adaptive 3D Semantic Segmentation Pipeline

Previous models [16, 20, 25] can only tackle a single adaptation task. As a pioneer work, UniDA3D tries to address multiple adaptation tasks in 3D segmentation field using a unified method and avoids the frequent adaptation method switching when facing different adaptation tasks or scenarios. UniDA3D is proposed to reduce the domain discrepancies from two aspects: 1) **Domain Active 3D Segmentation**, meaning that we actively mine a subset of source-and-target data that are representative and transferable for dynamically changing target-domain distribution, and 2) **Domain Adaptive 3D Segmentation**, meaning that we adapt a well-trained baseline to the target domain according to the above-sampled subset of the original data.

Domain Active 3D Segmentation: A Bi-domain Cross-modality Feature Interaction Module. Although inter-domain differences exist, we found that many frames in the source domain have a similar data distribution to those in the target domain. This phenomenon motivates us to mine target-domain-like frames from the source domain to enhance the model adaptability, regarded as **source-domain sampling**. On the other hand, for 3D segmentation scenarios, there are many semantically-duplicated samples between adjacent frames. To this end, to reduce the cost of target data acquisition and annotation, we propose to select a maximally-informative subset of a given unlabeled target domain to perform the pseudo-label or manual annotation process regarded as **target-domain sampling**.

In this part, we study how to design a unified sampling strategy to pick up samples from both domains, to reduce the feature gaps between domains and enhance the model

transferability. An effective method to alleviate the inter-domain data distribution differences of 3D point clouds is leveraging the multi-modality residing in the 3D segmentation dataset. Motivated by this, a cross-modality feature interaction module is exploited to train a domain discriminator that can dynamically evaluate the representativeness of each sample from image-point cloud modalities. Given a pair of images and point clouds (x_{2D}, x_{3D}) , the 2D and 3D backbones are respectively used to extract a pair of high-level features (f_{2D}, f_{3D}) , where $f_{2D} \in \mathbb{R}^{N \times F_{2D}}$ and $f_{3D} \in \mathbb{R}^{N \times F_{3D}}$. Although the feature pairs (f_{2D}, f_{3D}) extracted by the backbone network contain rich semantic information of a single modal, the cross-modal semantic relations between the images and point clouds are not taken into consideration.

Different from previous works [16, 25, 20] that align cross-modal features using a well-designed KL divergence loss, UniDA3D aims to exploit the relations between modalities by symmetrical attention [43]. This approach achieves better cross-modality feature interaction and thus is beneficial to pick up data representative for both image-and-point modalities. The feature maps from each modality $f \in \mathbb{R}^{N \times F_{2D}}$ can be described as $f = [f^1, f^2, \dots, f^N]$, where $f_{2D}^i \in \mathbb{R}^{F_{2D}}$ and $f_{3D}^i \in \mathbb{R}^{F_{3D}}$. In our implementation, the F_{2D} is equal to F_{3D} .

Given cross-modal feature pairs (f_{2D}, f_{3D}) and cross-modality feature interaction relations $(R_{3D \rightarrow 2D}, R_{2D \rightarrow 3D})$ (detailed calculation can be found in the Appendix), the enhanced representations can be written as follows:

$$\begin{aligned} \hat{f}_{2D} &= \text{FFN}(\text{Norm}(f_{2D} \odot R_{3D,2D})) , \\ \hat{f}_{3D} &= \text{FFN}(\text{Norm}(f_{3D} \odot R_{2D,3D})) , \end{aligned} \quad (3)$$

where \odot denotes an element-wise multiplication operation. And the FFN module allows the backbone to focus on the cross-branch modality discrepancies over the predicted semantically-similar regions. Overall, \hat{f}_{2D} and \hat{f}_{3D} are defined as the output features and will be concatenated and then fed into a well-designed domain discriminator, as illustrated in Fig. 2.

Furthermore, a 3-layer fully-convolutional domain discriminator \mathcal{D} with parameters θ_{Dis} is constructed, which takes the symmetrical-interaction features $[\hat{f}_{2D}, \hat{f}_{3D}]$ as input and is trained to distinguish the source data from the target ones. As shown in Fig. 3, the symmetrical-interaction features can take both 2D and 3D features into consideration, benefiting the training of the domain discriminator. We label the source domain and the target domain as '0' and '1', respectively. Let $\mathcal{L}_{\mathcal{D}}$ represent the domain classification loss of the discriminator. The training objective of the discriminator can be written as follows:

Algorithm 1: Source and Target Sampling Strategy

Input: A pair of high-level features $[f_{2D}, f_{3D}]$ extracted by 2D and 3D backbone. Domain discriminator \mathcal{D} for scoring pairs of data, containing cross-modality feature interaction module I_{cross} , sampling budget \mathcal{B} .

Output: The selected source or target set Z

- 1: $[\hat{f}_{2D}, \hat{f}_{3D}] = I_{cross}[f_{2D}, f_{3D}]$
- 2: $s_i = \mathcal{D}[\hat{f}_{2D}, \hat{f}_{3D}]$, where s_i denotes as i -th frame data containing point cloud and image pair from the source or target domain
- 3: Sort s_i in descending order
- 4: Sampling the data pairs according to the sorted s_i until budget \mathcal{B}_s or \mathcal{B}_t .
- 5: **return** Selected source or target set Z

$$\begin{aligned} \mathcal{L}_{Dis} = & \min_{\theta_{Dis}} \frac{1}{N^s} \sum_{x_{2D}^s, x_{3D}^s} \mathcal{L}_{\mathcal{D}}([\hat{f}_{2D}, \hat{f}_{3D}], 1) \\ & + \frac{1}{N^t} \sum_{x_{2D}^s, x_{3D}^s} \mathcal{L}_{\mathcal{D}}([\hat{f}_{2D}, \hat{f}_{3D}], 0). \end{aligned} \quad (4)$$

Once the trained domain discriminator is obtained, we can leverage the output of the domain discriminator to score each frame, which represents the domainness of a sample belonging to the source or target domain (see Algorithm 1). Since the active sampling strategy is one general approach, we can use it for both the source and target domain sampling. For the source domain, the higher score means that the frame complies with the distribution of the target domain. For the target domain, when the frame possesses the more informative characteristic, it will get a higher score. After the scoring stage is finished, all frames are sorted by the calculated scores, and the budget \mathcal{B}_s or \mathcal{B}_t frames are chosen as the sampled source data and target data.

Domain Adaptive 3D Segmentation: Effective Model Adaptation Strategy. When an informative subset jointly sampled from both source and target domains is determined, an effective adaptation strategy is designed to fully leverage these samples to enhance 3D segmentation model's adaptability. In this part, we investigate two representative target-oriented adaptation strategies to explore how to perform an effective model transfer based on these informative samples.

1) *Self-training using pseudo-labels:* Cross-modal learning is complementary to the pseudo-labeling technique, which is originally employed in semi-supervised and unsupervised domain adaptation tasks [19, 42]. In detail, given a pre-trained source model, the pseudo-labels can be obtained by selecting a portion of high-confidence predicted results according to the pre-trained model. It should be emphasized that the **Pseudo-Labeling methods (PL)** generate labels for the whole target domain data yet bring many label noises. By comparison, we can leverage the

UniDA3D to pick up samples with high domainness scores. Then, we only pseudo-label those selected samples to perform the subsequent self-training process. Such a sampling-based pseudo-labeling method is termed as **Active Pseudo-Labeling (APL)**. Based on those pseudo-labeled target frames, the model is further adapted to the target domain using the following segmentation loss:

$$\min_{\theta} \left[\frac{1}{|\mathcal{S}|} \sum_{\mathbf{x}^s} (\mathcal{L}_{seg}(\mathbf{x}^s, \mathbf{y}_{3D}^s)) + \frac{1}{|\mathcal{T}|} \sum_{\mathbf{x}^t} (\mathcal{L}_{seg}(\mathbf{x}^t, \hat{\mathbf{y}}_{3D})) \right], \quad (5)$$

where $\hat{\mathbf{y}}_{3D}$ represents the pseudo-labels.

2) *Off-the-shelf UDA techniques:* Furthermore, our sampling strategy can be easily integrated into the existing methods, such as xMUDA [16], AUDA [20], and the state-of-the-art DsCML [25], to further boost their cross-domain segmentation accuracy. Specifically, we first utilize the proposed sampling strategy to pick up the maximally-informative samples from both source and target domains and construct a new subset. Then, these UDA-based techniques are employed to adapt the baseline model using the newly-constructed subset to achieve a more effective and safe model adaptation.

4. Experiments

4.1. Dataset Description

Our UniDA3D is evaluated under 3 real-to-real adaptation tasks and 1 virtual-to-real adaptation task. The first task is the day-to-night adaptation, which presents a domain gap caused by the illumination changes, where the laser beams are almost invariant to illumination conditions while the camera suffers from a low-light environment. The second task is the country-to-country adaptation, representing a large domain difference where the 3D shapes and images might change frequently. The third task is the dataset-to-dataset adaptation, containing the variations in the sensor setup. The last task is the virtual-to-real adaptation with huge domain gaps existing in it. The widely-used autonomous driving datasets nuScenes [3], A2D2 [10], and SemanticKITTI [1] are utilized, where the LiDAR and camera are synchronized and calibrated to obtain the projection between a 3D point and its corresponding 2D image pixel. All these datasets consist of 3D annotations. And only the front camera images and the LiDAR points are utilized for simplicity and consistency across datasets. For nuScenes, the point-wise labels for 3D semantic segmentation are obtained by assigning the corresponding object label if that point lies inside an annotated 3D bounding box. If not, that point will be labeled as background. Following the works [16, 25], two scenarios of Day/Night and USA/Singapore are conducted. For the adaptation from A2D2 to SemanticKITTI,

	Methods	USA/Singapore			Day/Night			A2D2/SemanticKITTI			V-KITTI/SemanticKITTI		
		2D	3D	Softmax Avg.	2D	3D	Softmax Avg.	2D	3D	Softmax Avg.	2D	3D	Softmax Avg.
Domain adaptation methods	Oracle	66.4	63.8	71.6	48.6	47.1	55.2	58.3	71.0	73.7	66.3	78.4	80.1
	MinEnt (CVPR-19)[35]	53.4	47.0	59.7	44.9	43.5	51.3	38.8	38.0	42.7	37.8	39.6	42.6
	PL (CVPR-19) [19]	55.5	51.8	61.5	43.7	45.1	48.6	37.4	44.8	47.7	21.5	44.3	35.6
	CyCADA (ICML-18) [13]	54.9	48.7	61.4	45.7	45.2	49.7	38.2	44.3	43.9	-	-	-
	AdaptSegNet (CVPR-18) [34]	56.3	47.7	61.8	45.3	44.6	49.6	38.8	44.3	44.2	-	-	-
	CLAN (CVPR-19) [21]	57.8	51.2	62.5	45.6	43.7	49.2	39.2	44.7	44.5	-	-	-
	xMUDA (CVPR-20) [16]	59.3	52.0	62.7	46.2	44.2	50.0	36.8	43.3	42.9	42.1	46.7	48.2
	xMUDA + PL (CVPR-20) [16]	61.1	54.1	63.2	47.1	46.7	50.8	43.7	48.5	49.1	45.8	51.4	52.0
	AUDA [20]	59.7	51.7	63.0	48.7	46.2	55.7	43.3	43.3	47.3	41.4	47.7	49.3
	AUDA + PL [20]	59.8	52.0	63.1	49.0	47.6	54.2	43.0	43.6	46.8	41.6	53.1	51.2
	DsCML (CVPR-21) [25]	61.3	53.3	63.6	48.0	45.7	51.0	39.6	45.1	44.5	46.2	42.9	49.9
Sampling source-domain w/ UniDA3D	DsCML + CMAL (CVPR-21) [25]	63.4	55.6	64.8	49.5	48.2	52.7	46.3	50.7	51.0	47.6	43.1	51.2
	DsCML + CMAL + PL (CVPR-21) [25]	63.9	56.3	65.1	50.1	48.7	53.0	46.8	51.8	52.4	48.1	44.4	52.6
UDA task w/ UniDA3D	Source only	53.4	46.5	61.3	42.2	41.2	47.8	34.2	35.9	40.4	26.8	42.0	42.2
	Source only + Source-domain sampling	55.2	49.7	63.1	45.4	40.8	51.7	35.1	38.0	44.7	33.0	44.2	45.1
	<i>Improvement</i>	+1.8	+3.2	+1.8	+3.2	+0.4	+3.9	+0.9	+2.1	+4.3	+6.2	+2.2	+2.9
	Source only + Source-domain sampling + PL	59.4	53.6	63.3	46.2	42.6	51.4	42.0	35.9	45.8	34.4	44.7	47.5
	<i>Improvement</i>	+5.0	+7.1	+2.0	+4.0	+1.4	+3.6	+7.8	+5.4	+5.4	+7.6	+2.7	+5.3
	Source only + Source-domain sampling + APL	60.9	53.1	66.8	47.0	42.2	51.9	41.9	41.4	46.7	36.2	40.8	46.8
	<i>Improvement</i>	+7.5	+6.6	+5.5	+4.8	+1.0	+3.1	+7.7	+5.5	+6.3	+10.2	-1.2	+4.6
	xMUDA + Source-domain sampling	55.9	50.1	63.4	45.6	42.2	51.2	43.6	47.6	50.8	44.0	50.8	54.8
	<i>Improvement</i>	-	-	+0.7	-	-	+1.2	-	-	+7.9	-	-	+2.6
	xMUDA + Source-domain sampling + PL	60.8	51.4	63.6	46.2	42.6	51.4	42.7	43.3	50.6	42.5	51.4	56.6
	<i>Improvement</i>	-	-	+0.6	-	-	+1.4	-	-	+1.5	-	-	+4.6
	xMUDA + Source-domain sampling + APL	57.6	54.6	63.8	48.4	42.8	51.5	45.1	46.3	50.6	47.4	50.8	56.7
	<i>Improvement</i>	-	-	+0.6	-	-	+0.7	-	-	+1.5	-	-	+4.7
UDA task w/ UniDA3D	AUDA + Source-domain sampling	54.7	50.3	63.2	49.1	48.4	54.4	43.7	42.3	47.0	46.2	52.7	54.3
	<i>Improvement</i>	-	-	+0.0	-	-	+0.2	-	-	+0.2	-	-	+5.0
	AUDA + Source-domain sampling + PL	59.4	53.9	63.3	49.1	41.3	54.0	42.6	37.9	47.1	48.3	52.5	54.2
	<i>Improvement</i>	-	-	+0.1	-	-	-0.2	-	-	+0.3	-	-	+3.0
	AUDA + Source-domain sampling + APL	58.3	52.4	63.6	48.5	41.6	54.7	42.0	39.7	47.9	45.7	53.7	54.9
	<i>Improvement</i>	-	-	+0.5	-	-	-0.5	-	-	+1.1	-	-	+3.7
	DsCML + CMAL + Source-domain sampling	55.6	52.0	65.0	49.3	41.6	53.5	43.5	46.3	51.1	52.9	49.5	53.0
	<i>Improvement</i>	-	-	+0.2	-	-	+0.8	-	-	+0.1	-	-	+1.8
	DsCML + CMAL + Source-domain sampling + PL	59.9	55.2	65.7	49.1	41.5	53.3	44.7	47.0	52.7	52.6	51.1	56.5
	<i>Improvement</i>	-	-	+0.6	-	-	+0.3	-	-	+0.3	-	-	+5.3
UFDA task w/ UniDA3D	DsCML + CMAL + Source-domain sampling + APL	61.8	55.7	66.2	49.2	42.6	53.4	47.3	46.1	54.3	52.3	53.0	56.7
	<i>Improvement</i>	-	-	+1.1	-	-	+0.4	-	-	+1.9	-	-	+5.5
UFDA task w/ UniDA3D	UFDA (10% target samples)	55.0	49.3	63.0	45.1	41.0	51.3	35.0	37.9	44.2	31.7	43.8	44.3
	UFDA (5% target samples)	54.6	48.9	62.2	43.7	40.7	50.5	34.5	37.2	43.6	30.9	40.2	40.7

Table 1. Segmentation results (mIoU) for different adaptation tasks including UDA task, UDA methods coupled with UniDA3D, and UFDA task, using four multi-modal domain adaptation scenarios. “V-KITTI” denotes the VirtualKITTI dataset, and “Avg.” represents the performance which is obtained by computing the mean of the predicted 2D and 3D probabilities after softmax operation. “PL” denotes the pseudo-labeling operation for all target data, while “APL” is proposed to pseudo-label the actively sampled target-domain data.

the point-wise labels on A2D2 are directly provided, and the 10 categories shared between the two datasets are selected. To compensate for source/target class mismatch (e.g., VirtualKITTI/SemanticKITTI) or accommodate for class scarcity, a custom class mapping is applied, which is detailed in Appendix. Note that VirtualKITTI provides depth maps so that we can simulate LiDAR scanning via the uniform point sampling.

4.2. The Designed Baselines

In order to validate the effectiveness of our UniDA3D, 7 baselines are designed: **Baseline 1** only leverages 2D features extracted by the 2D backbone. The 2D scores obtained by the domain discriminator \mathcal{D} are used to sample the source and target data. **Baseline 2** utilizes the 3D features for sampling, where the sampling process will depend on the 3D scores from the \mathcal{D} . **Baseline 3** naively averages the 2D and 3D scores for the sampling strategy. Since the scores are calculated from a single modality, the sampled data might be distributed in a single modality. For instance, the data sampled by the 2D scores will concentrate more on the image information and vice versa. **Baseline 4** integrates the 2D active domain adaptation method CLUE [6], to be

compared with our UniDA3D in 3D semantic segmentation. **Baseline 5** further applies the LabOR [29] (a representative method for active segmentation model) to pick up data from the target domain. **Baseline 6** uses 2D to 3D interaction to obtain the \hat{f}_{3D} , while **Baseline 7** utilizes 2D to 3D interaction to obtain the \hat{f}_{2D} . \hat{f}_{2D} and \hat{f}_{3D} will be leveraged for scoring by the domain discriminator \mathcal{D} . The module-wise ablation study of all these baselines can be found in Table 3, and please refer to the Appendix for the network visualization of all designed baselines.

4.3. Implementation Details

Network Backbone. For a fair comparison with the state-of-the-art multi-modal 3D domain adaptation frameworks, we leverage the ResNet34 [12] pre-trained on ImageNet [9] as the encoder for the 2D network branch and the SparseConvNet [11] with U-Net architecture for 3D network branch. Moreover, the voxel size is set to 5 cm in the 3D network to ensure that only one 3D point lies in a single voxel. The models are trained and evaluated with PyTorch toolbox [24]. We train UniDA3D with one Tesla A100 GPU.

Parameter Settings. In the training stage, the batch size is set to 8, and the Adaptive Moment Estimation (Adam) [18]

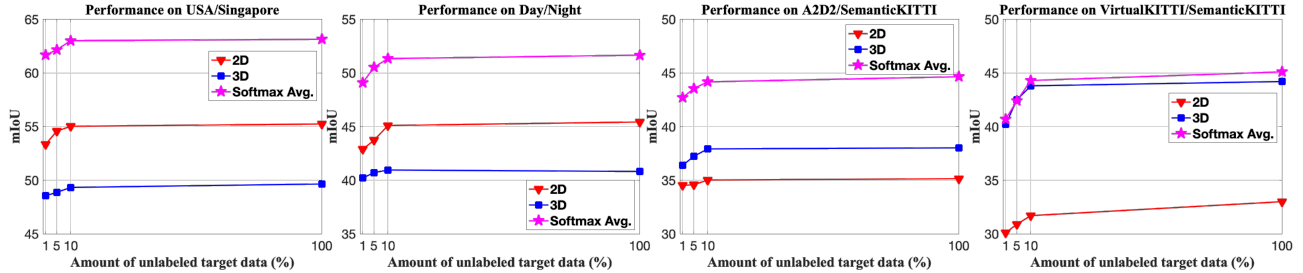


Figure 4. Segmentation results (mIoU) under the UFDA task, where we study the adaptation performance under different amounts of samples from the target domain: 100%, 10%, 5%, and 1% target domain samples.

	Methods	USA/Singapore			Day/Night			A2D2/SemanticKITTI			VirtualKITTI/SemanticKITTI		
		2D	3D	Softmax Avg.	2D	3D	Softmax Avg.	2D	3D	Softmax Avg.	2D	3D	Softmax Avg.
	Source only	53.4	46.5	61.3	42.2	41.2	47.8	34.2	35.9	40.4	26.8	42.0	42.2
UDA	xMUDA + PL [16]	61.1	54.1	63.2	47.1	46.7	50.8	43.7	48.5	49.1	45.8	51.4	52.0
	AUDA + PL [20]	59.8	52.0	63.1	49.0	47.6	54.2	43.0	43.6	46.8	41.6	53.1	51.2
	DsCML + CMAL + PL [25]	63.9	56.3	65.1	50.1	48.7	53.0	46.8	51.8	52.4	47.6	43.1	51.2
ADA	Ours + Source-domain sampling	55.2	49.7	63.1	45.4	40.8	51.7	35.1	38.0	44.7	33.0	44.2	45.1
	Ours + Random sampling (Target domain)	55.5	58.7	64.9	47.5	41.0	53.0	42.8	43.1	48.2	45.6	52.1	57.9
	Ours + Source-domain sampling + Target-domain sampling	63.6	52.8	67.4	47.1	41.5	53.6	43.9	47.8	51.1	49.3	52.1	58.5
	Ours + Source-domain sampling + Target-domain sampling + APL	62.7	56.3	68.1	49.8	41.2	54.6	46.2	45.7	52.8	51.8	53.7	59.2
	Oracle	66.4	63.8	71.6	48.6	47.1	55.2	58.3	71.0	73.7	66.3	78.4	80.1

Table 2. Segmentation results (mIoU) for the ADA task under 5% target-domain annotation budget \mathcal{B}_t , where Random sampling denotes that we randomly sample 5% target domain to perform the manual annotation.

is used as the optimizer with $\beta_1 = 0.9$ and $\beta_2 = 0.999$. We set the learning rate of $1 \times e^{-3}$ initially and follow the poly learning rate policy [5] with a poly power of 0.9. We set the max training iteration as 100k.

4.4. Experimental Results

In this part, we conduct experiments on UDA, UFDA, and ADA tasks, and comprehensively show the generality and effectiveness in addressing 3D segmentation model’s domain discrepancies.

Results on 3D UDA task. 1) *The effectiveness of source-domain sampling:* As shown in Table 1, when the segmentation baseline model is deployed to a new domain (*e.g.*, from USA to Singapore), its segmentation accuracy is seriously degraded (only 61.3% compared with 71.6% achieved by fully-supervised model). One cost-free solution provided by our UniDA3D is to use the designed source-domain sampling strategy, which can actually sample some target-domain-like source data to bridge the large domain shift from different modal data, achieving 1.8%, 3.9%, 4.3%, and 2.9% accuracy gains for different cross-domain scenarios. The accuracy gain achieved by only source sampling strategy even surpasses some representative uni-modal UDA methods such as MinEnt [35], PL [19], CyCADA [13], AdaptSegNet [34], and CLAN [21].

Furthermore, we would like to emphasize that another advantage of our UniDA3D is that it can be plugged and played into the existing UDA models (*e.g.*, xMUDA [16], AUDA [20], and DsCML [25]), to further strengthen these UDA models’ adaptability. For example, xMUDA coupled

with our UniDA3D achieves 0.7%, 1.2%, 7.9%, and 2.6% segmentation accuracy gain compared with xMUDA itself, for the USA/Singapore, Day/Night, A2D2/SemanticKITTI, and VirtualKITTI/SemanticKITTI scenarios. Also, we conduct extensive validations by inserting our UniDA3D into many UDA models, such as AUDA [20] and DsCML [25], and observe consistent segmentation accuracy gains.

2) *The effectiveness of target-domain sampling:* APL means that we only perform the pseudo-labeling process for the selected target samples by UniDA3D. Also, it can be seen from Table 1 that, compared with the widely-used Pseudo-Labeling (PL) strategy, APL can obtain a relatively high mIoU in A2D2/SemanticKITTI setting. This is mainly because the selected target data (SemanticKITTI) by UniDA3D presents less noise and can be pseudo-labeled more accurately. By merging the merits of the APL and self-training strategy, UniDA3D can further enhance the adaptability of the model.

Results on 3D UFDA task. Motivated by the outstanding performance of UniDA3D in UDA task, we try to reduce the number of unlabeled target data to check the domain-related representation ability of the designed discriminator with the cross-modality feature interaction module. Such a task setting can be regarded as UFDA task. Specifically, we randomly select a small number of target data (*e.g.* 10%, 5%, and even 1%) to train the discriminator, and the results are shown in Fig. 4. It can be seen that owing to the robust source-domain sampling strategy, only a few-shot unlabeled target data also can effectively train the designed discriminator and achieve a comparable target-domain segmentation

Methods	USA/Singapore			Day/Night			A2D2/SemanticKITTI			VirtualKITTI/SemanticKITTI		
	2D	3D	Softmax Avg.	2D	3D	Softmax Avg.	2D	3D	Softmax Avg.	2D	3D	Softmax Avg.
Baseline1: UniDA3D-2D	55.2	47.1	62.8	45.2	40.9	50.6	34.8	36.6	43.0	36.2	40.6	44.9
Baseline2: UniDA3D-3D	53.8	48.8	61.8	44.9	41.2	51.0	35.5	38.4	42.7	31.7	40.8	44.6
Baseline3: UniDA3D-2D-3D-Avg	53.4	48.9	61.8	45.0	41.2	51.1	35.7	36.9	43.2	35.2	40.5	45.0
Baseline4: UniDA3D-CLUE [6]	53.2	46.3	60.1	42.8	41.0	49.4	35.2	36.0	40.6	31.2	40.4	42.7
Baseline5: UniDA3D-LabOR [29]	52.2	50.0	58.9	44.0	40.1	49.2	31.3	32.0	38.6	33.1	40.1	43.4
Baseline6: UniDA3D-2D-to-3D-Interaction	57.9	49.7	60.7	43.0	41.8	50.3	34.4	36.1	42.1	32.4	44.6	42.8
Baseline7: UniDA3D-3D-to-2D-Interaction	56.8	46.5	62.2	45.3	42.2	51.3	35.0	35.0	42.1	35.2	40.8	44.3
Ours: UniDA3D-Symmetrical-Interaction	55.2	49.7	63.1	45.4	40.8	51.7	35.1	38.0	44.7	33.0	44.2	45.1

Table 3. The module-level ablation studies of UniDA3D under four multi-modal domain adaptation scenarios.

accuracy, providing an option to eliminate the need for unlabeled target data.

Results on 3D ADA task. In the above DA tasks, all samples from the target domain are unlabeled. Although performing the APL or PL based on self-training methods on the unlabeled target domain can improve the target-domain segmentation accuracy, there is still a large accuracy gap between the unsupervised target-domain model and the fully-supervised one. To this end, in this work, we also study the ADA task, which assumes that a portion of unlabeled target data selected by an active learning algorithm can be annotated by an oracle or human expert. Instead of using pseudo-labeled target samples, we utilize an oracle to annotate all selected target samples to investigate if our UniDA3D can be applied to ADA task.

As shown in Table 2, the baseline model fine-tuned on the sampled source data and annotated target data can significantly enhance the model transferability, obtaining 67.4%, 53.6%, 51.1%, and 58.4% segmentation accuracies under different settings. Furthermore, we conduct experiments on changing the budget of the target-domain annotation. The results can be found in Fig. 5, and we observe that the model performance in the target domain is improved with the increase of the annotation budget. We also observe that the 5% annotation budget can be regarded as a good trade-off between the annotation cost and the model adaptability.

4.5. Further Analyses

Module-level Ablation Studies. To validate the effectiveness of the symmetrical attention module, ablation studies are conducted to gain insight into the symmetrical attention module. As shown in Table 3, the sampled source data by only the 2D scores tend to boost the accuracy of baseline on 2D metric, while the samples selected only by 3D scores are more beneficial to improve the 3D segmentation results. When the mean sampling strategy (**Baseline 3**) is utilized, the average accuracy is able to be improved. By employing the designed symmetrical attention module, satisfactory overall results can be obtained, showing the effectiveness and strength of our symmetrical attention-based sampling strategy.

Segmentation Accuracy for Both Domains. To validate

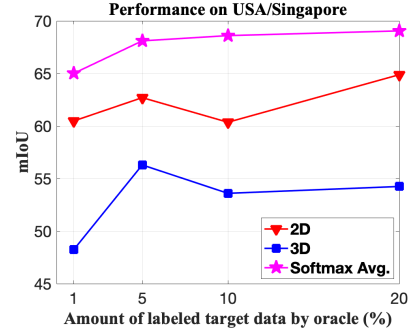


Figure 5. The influence of different target-domain annotation budget \mathcal{B}_t (20%, 10%, 5%, and 1%) on the ADA task. Here, we take the USA-to-Singapore setting for an example.

	Source	Target	Average
	2D / 3D / Avg.	2D / 3D / Avg.	2D / 3D / Avg.
Source only	53.4 / 46.5 / 61.3	31.4 / 43.4 / 49.1	42.4 / 45.0 / 55.2
xMUDA	36.6 / 43.8 / 48.6	55.9 / 50.1 / 63.4	46.3 / 47.0 / 56.0
UniDA3D	47.8 / 43.1 / 54.9	63.6 / 52.8 / 67.4	55.7 / 48.0 / 61.2

Table 4. Generalization ability of UniDA3D. The results tested on both source and target domains are reported. Avg. denotes the softmax average performance.

the multi-domain generalization ability of our UniDA3D, further experiments are conducted to observe the segmentation accuracy of the model on both source and target domains. As shown in Table 4, the source-only baseline, which means that the model is trained only on the source domain and directly tested on the target domain, has the best segmentation accuracy for the source domain, but it is hard to be generalized to the target domain. On the other hand, the xMUDA baseline (UDA model) achieves better results on the target domain but not performs well on the source domain. Our UniDA3D performs a fine-tuning process on the selected source data (labeled) and the target data (pseudo-labeled or annotated), achieving better generalization on both the source and target domains.

5. Conclusion

In this paper, we have presented a UniDA3D to tackle many adaptation tasks, including UDA, UFDA, and ADA tasks, by means of a unified pipeline. By the merits of the designed bi-domain cross-modality feature interaction module, UniDA3D can fully leverage features from differ-

ent modalities to achieve an informative sample selection process from different domains. Experiments are conducted on widely-used 3D semantic segmentation datasets, showing the superiority of UniDA3D in boosting the segmentation model transferability.

Acknowledgement

This work is supported by Science and Technology Commission of Shanghai Municipality (grant No. 22DZ1100102).

References

- [1] Jens Behley, Martin Garbade, Andres Milioto, Jan Quenzel, Sven Behnke, Cyrill Stachniss, and Jürgen Gall. Semantickitti: A dataset for semantic scene understanding of lidar sequences. In *Proceedings of the IEEE/CVF international conference on computer vision*, pages 9297–9307, 2019. [1](#), [2](#), [5](#)
- [2] Jan-Aike Bolte, Markus Kamp, Antonia Breuer, Silviu Homoeanu, Peter Schlicht, Fabian Huger, Daniel Lipinski, and Tim Fingscheidt. Unsupervised domain adaptation to improve image segmentation quality both in the source and target domain. In *Proceedings of the IEEE/CVF Conference on Computer Vision and Pattern Recognition Workshops*, pages 0–0, 2019. [1](#)
- [3] Holger Caesar, Varun Bankiti, Alex H Lang, Sourabh Vora, Venice Erin Liang, Qiang Xu, Anush Krishnan, Yu Pan, Giacarlo Baldan, and Oscar Beijbom. nuscenes: A multimodal dataset for autonomous driving. In *Proceedings of the IEEE/CVF conference on computer vision and pattern recognition*, pages 11621–11631, 2020. [1](#), [2](#), [5](#), [13](#)
- [4] Rita Chattopadhyay, Wei Fan, Ian Davidson, Sethuraman Panchanathan, and Jieping Ye. Joint transfer and batch-mode active learning. In *International conference on machine learning*, pages 253–261. PMLR, 2013. [2](#)
- [5] Liang-Chieh Chen, George Papandreou, Florian Schroff, and Hartwig Adam. Rethinking atrous convolution for semantic image segmentation. *arXiv preprint arXiv:1706.05587*, 2017. [7](#)
- [6] Yixin Chen, James Ze Wang, and Robert Krovetz. Clue: Cluster-based retrieval of images by unsupervised learning. *IEEE transactions on Image Processing*, 14(8):1187–1201, 2005. [6](#), [8](#)
- [7] Christopher Choy, JunYoung Gwak, and Silvio Savarese. 4d spatio-temporal convnets: Minkowski convolutional neural networks. In *Proceedings of the IEEE/CVF conference on computer vision and pattern recognition*, pages 3075–3084, 2019. [2](#)
- [8] Yuhang Ding, Xin Yu, and Yi Yang. Modeling the probabilistic distribution of unlabeled data for one-shot medical image segmentation. In *Proceedings of the AAAI conference on artificial intelligence*, volume 35, pages 1246–1254, 2021. [1](#)
- [9] Yaroslav Ganin and Victor Lempitsky. Unsupervised domain adaptation by backpropagation. In *International conference on machine learning*, pages 1180–1189. PMLR, 2015. [6](#), [12](#)
- [10] Jakob Geyer, Yohannes Kassahun, Mentar Mahmudi, Xavier Ricou, Rupesh Durgesh, Andrew S Chung, Lorenz Hauswald, Viet Hoang Pham, Maximilian Mühlegg, Sebastian Dorn, et al. A2d2: Audi autonomous driving dataset. *arXiv preprint arXiv:2004.06320*, 2020. [2](#), [5](#)
- [11] Benjamin Graham, Martin Engelcke, and Laurens Van Der Maaten. 3d semantic segmentation with submanifold sparse convolutional networks. In *Proceedings of the IEEE conference on computer vision and pattern recognition*, pages 9224–9232, 2018. [1](#), [2](#), [3](#), [6](#)
- [12] Kaiming He, Xiangyu Zhang, Shaoqing Ren, and Jian Sun. Deep residual learning for image recognition. In *Proceedings of the IEEE conference on computer vision and pattern recognition*, pages 770–778, 2016. [3](#), [6](#)
- [13] Judy Hoffman, Eric Tzeng, Taesung Park, Jun-Yan Zhu, Phillip Isola, Kate Saenko, Alexei Efros, and Trevor Darrell. Cycada: Cycle-consistent adversarial domain adaptation. In *International conference on machine learning*, pages 1989–1998. Pmlr, 2018. [6](#), [7](#)
- [14] Wenbo Hu, Hengshuang Zhao, Li Jiang, Jiaya Jia, and Tien-Tsin Wong. Bidirectional projection network for cross dimension scene understanding. In *Proceedings of the IEEE/CVF Conference on Computer Vision and Pattern Recognition*, pages 14373–14382, 2021. [1](#)
- [15] Zeyu Hu, Xuyang Bai, Jiaxiang Shang, Runze Zhang, Jiayu Dong, Xin Wang, Guangyuan Sun, Hongbo Fu, and Chiew-Lan Tai. Vmnet: Voxel-mesh network for geodesic-aware 3d semantic segmentation. In *Proceedings of the IEEE/CVF International Conference on Computer Vision*, pages 15488–15498, 2021. [2](#)
- [16] Maximilian Jaritz, Tuan-Hung Vu, Raoul de Charette, Emilie Wirbel, and Patrick Pérez. xmuda: Cross-modal unsupervised domain adaptation for 3d semantic segmentation. In *Proceedings of the IEEE/CVF conference on computer vision and pattern recognition*, pages 12605–12614, 2020. [1](#), [2](#), [3](#), [4](#), [5](#), [6](#), [7](#), [12](#)
- [17] Maximilian Jaritz, Tuan-Hung Vu, Raoul De Charette, Émilie Wirbel, and Patrick Pérez. Cross-modal learning for domain adaptation in 3d semantic segmentation. *IEEE Transactions on Pattern Analysis and Machine Intelligence*, 45(2):1533–1544, 2022. [2](#)
- [18] Diederik P Kingma and Jimmy Ba. Adam: A method for stochastic optimization. *arXiv preprint arXiv:1412.6980*, 2014. [6](#)
- [19] Yunsheng Li, Lu Yuan, and Nuno Vasconcelos. Bidirectional learning for domain adaptation of semantic segmentation. In *Proceedings of the IEEE/CVF Conference on Computer Vision and Pattern Recognition*, pages 6936–6945, 2019. [5](#), [6](#), [7](#)
- [20] Wei Liu, Zhiming Luo, Yuanzheng Cai, Ying Yu, Yang Ke, José Marcato Junior, Wesley Nunes Gonçalves, and Jonathan Li. Adversarial unsupervised domain adaptation for 3d semantic segmentation with multi-modal learning. *ISPRS Journal of Photogrammetry and Remote Sensing*, 176:211–221, 2021. [1](#), [2](#), [3](#), [4](#), [5](#), [6](#), [7](#)
- [21] Yawei Luo, Liang Zheng, Tao Guan, Junqing Yu, and Yi Yang. Taking a closer look at domain shift: Category-level

- adversaries for semantics consistent domain adaptation. In *Proceedings of the IEEE/CVF Conference on Computer Vision and Pattern Recognition*, pages 2507–2516, 2019. 6, 7
- [22] Ke Mei, Chuang Zhu, Jiaqi Zou, and Shanghang Zhang. Instance adaptive self-training for unsupervised domain adaptation. In *Computer Vision–ECCV 2020: 16th European Conference, Glasgow, UK, August 23–28, 2020, Proceedings, Part XXVI 16*, pages 415–430. Springer, 2020. 2
- [23] A Tuan Nguyen, Toan Tran, Yarin Gal, and Atilim Gunes Baydin. Domain invariant representation learning with domain density transformations. *Advances in Neural Information Processing Systems*, 34:5264–5275, 2021. 1
- [24] Adam Paszke, Sam Gross, Soumith Chintala, Gregory Chanan, Edward Yang, Zachary DeVito, Zeming Lin, Alban Desmaison, Luca Antiga, and Adam Lerer. Automatic differentiation in pytorch. *Openreview*, 2017. 6
- [25] Duo Peng, Yinjie Lei, Wen Li, Pingping Zhang, and Yulan Guo. Sparse-to-dense feature matching: Intra and inter domain cross-modal learning in domain adaptation for 3d semantic segmentation. In *Proceedings of the IEEE/CVF International Conference on Computer Vision*, pages 7108–7117, 2021. 1, 2, 3, 4, 5, 6, 7
- [26] Charles Ruizhongtai Qi, Li Yi, Hao Su, and Leonidas J Guibas. Pointnet++: Deep hierarchical feature learning on point sets in a metric space. *Advances in neural information processing systems*, 30, 2017. 2
- [27] Piyush Rai, Avishek Saha, Hal Daumé III, and Suresh Venkatasubramanian. Domain adaptation meets active learning. In *Proceedings of the NAACL HLT 2010 Workshop on Active Learning for Natural Language Processing*, pages 27–32, 2010. 2
- [28] Pengzhen Ren, Yun Xiao, Xiaojun Chang, Po-Yao Huang, Zhihui Li, Brij B Gupta, Xiaojiang Chen, and Xin Wang. A survey of deep active learning. *ACM computing surveys (CSUR)*, 54(9):1–40, 2021. 2
- [29] Inkyu Shin, Dong-Jin Kim, Jae Won Cho, Sanghyun Woo, Kwanyong Park, and In So Kweon. Labor: Labeling only if required for domain adaptive semantic segmentation. In *Proceedings of the IEEE/CVF International Conference on Computer Vision*, pages 8588–8598, 2021. 6, 8, 12
- [30] Vishwanath A Sindagi and Vishal M Patel. Ha-ccn: Hierarchical attention-based crowd counting network. *IEEE Transactions on Image Processing*, 29:323–335, 2019. 1
- [31] Jong-Chyi Su, Yi-Hsuan Tsai, Kihyuk Sohn, Buyu Liu, Subhransu Maji, and Manmohan Chandraker. Active adversarial domain adaptation. In *Proceedings of the IEEE/CVF Winter Conference on Applications of Computer Vision*, pages 739–748, 2020. 2
- [32] Hugues Thomas, Charles R Qi, Jean-Emmanuel Deschaud, Beatriz Marcotegui, François Goulette, and Leonidas J Guibas. Kpconv: Flexible and deformable convolution for point clouds. In *Proceedings of the IEEE/CVF international conference on computer vision*, pages 6411–6420, 2019. 2
- [33] Marco Toldo, Andrea Maracani, Umberto Michieli, and Pietro Zanuttigh. Unsupervised domain adaptation in semantic segmentation: a review. *Technologies*, 8(2):35, 2020. 1
- [34] Yi-Hsuan Tsai, Wei-Chih Hung, Samuel Schulter, Ki-hyuk Sohn, Ming-Hsuan Yang, and Manmohan Chandraker. Learning to adapt structured output space for semantic segmentation. In *Proceedings of the IEEE conference on computer vision and pattern recognition*, pages 7472–7481, 2018. 6, 7
- [35] Tuan-Hung Vu, Himalaya Jain, Maxime Bucher, Matthieu Cord, and Patrick Pérez. Advent: Adversarial entropy minimization for domain adaptation in semantic segmentation. In *Proceedings of the IEEE/CVF Conference on Computer Vision and Pattern Recognition*, pages 2517–2526, 2019. 6, 7
- [36] Lei Wang, Yuchun Huang, Yaolin Hou, Shenman Zhang, and Jie Shan. Graph attention convolution for point cloud semantic segmentation. In *Proceedings of the IEEE/CVF conference on computer vision and pattern recognition*, pages 10296–10305, 2019. 1
- [37] Shenlong Wang, Simon Suo, Wei-Chiu Ma, Andrei Pokrovsky, and Raquel Urtasun. Deep parametric continuous convolutional neural networks. In *Proceedings of the IEEE conference on computer vision and pattern recognition*, pages 2589–2597, 2018. 2
- [38] Yue Wang, Yongbin Sun, Ziwei Liu, Sanjay E Sarma, Michael M Bronstein, and Justin M Solomon. Dynamic graph cnn for learning on point clouds. *AcM Transactions On Graphics (tog)*, 38(5):1–12, 2019. 2
- [39] Zhonghao Wang, Mo Yu, Yunchao Wei, Rogerio Feris, Jin-jun Xiong, Wen-mei Hwu, Thomas S Huang, and Honghui Shi. Differential treatment for stuff and things: A simple unsupervised domain adaptation method for semantic segmentation. In *Proceedings of the IEEE/CVF Conference on Computer Vision and Pattern Recognition*, pages 12635–12644, 2020. 1
- [40] Garrett Wilson and Diane J Cook. A survey of unsupervised deep domain adaptation. *ACM Transactions on Intelligent Systems and Technology (TIST)*, 11(5):1–46, 2020. 1
- [41] Shuquan Ye, Dongdong Chen, Songfang Han, and Jing Liao. Learning with noisy labels for robust point cloud segmentation. In *Proceedings of the IEEE/CVF International Conference on Computer Vision*, pages 6443–6452, 2021. 2
- [42] Yu-Ting Yen, Chia-Ni Lu, Wei-Chen Chiu, and Yi-Hsuan Tsai. 3d-pl: Domain adaptive depth estimation with 3d-aware pseudo-labeling. In *European Conference on Computer Vision*, pages 710–728. Springer, 2022. 5
- [43] Bo Zhang, Jiakang Yuan, Baopu Li, Tao Chen, Jiayuan Fan, and Botian Shi. Learning cross-image object semantic relation in transformer for few-shot fine-grained image classification. In *Proceedings of the 30th ACM International Conference on Multimedia*, pages 2135–2144, 2022. 4
- [44] Kuangen Zhang, Ming Hao, Jing Wang, Clarence W de Silva, and Chenglong Fu. Linked dynamic graph cnn: Learning on point cloud via linking hierarchical features. *arXiv preprint arXiv:1904.10014*, 2019. 2
- [45] Pan Zhang, Bo Zhang, Ting Zhang, Dong Chen, Yong Wang, and Fang Wen. Prototypical pseudo label denoising and target structure learning for domain adaptive semantic segmentation. In *Proceedings of the IEEE/CVF conference on com-*

- puter vision and pattern recognition*, pages 12414–12424, 2021. 2
- [46] Qiming Zhang, Jing Zhang, Wei Liu, and Dacheng Tao. Category anchor-guided unsupervised domain adaptation for semantic segmentation. *Advances in neural information processing systems*, 32, 2019. 1
 - [47] Yang Zou, Zhiding Yu, BVK Kumar, and Jinsong Wang. Unsupervised domain adaptation for semantic segmentation via class-balanced self-training. In *Proceedings of the European conference on computer vision (ECCV)*, pages 289–305, 2018. 2

A. Details on Cross-modality Feature Interaction

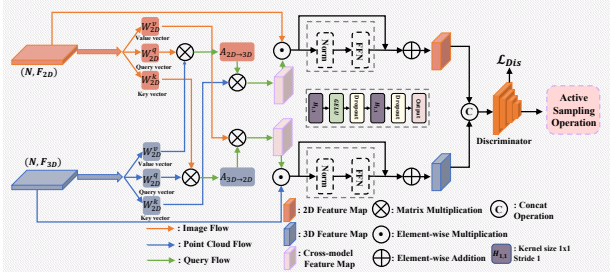


Figure 5. The illustration of cross-modality feature interaction module.

Given feature maps with weight parameters $W_{2D}^q, W_{2D}^k, W_{2D}^v$ for the image branch $2D$, and parameters $W_{3D}^q, W_{3D}^k, W_{3D}^v$ for point cloud branch $3D$, the query vector q^i , key vector k^i , and value vector v^i can be calculated as follows:

$$q_{2D} := W_{2D}^q f_{2D}^i, \quad k_{2D} := W_{2D}^k f_{2D}^i, \quad v_{2D} := W_{2D}^v f_{2D}^i, \quad (6)$$

$$q_{3D} := W_{3D}^q f_{3D}^i, \quad k_{3D} := W_{3D}^k f_{3D}^i, \quad v_{3D} := W_{3D}^v f_{3D}^i. \quad (7)$$

After that, the symmetrical cross-attention is leveraged in a bi-directional manner: 1) The $2D$ branch-related features are obtained using the value vector v_{3D}^i from $3D$ backbone branch, formulated as $3D \rightarrow 2D$; 2) Similarly, the $3D$ branch-related features are acquired using the value vector v_{2D}^i of the $2D$ backbone branch, formulated as $2D \rightarrow 3D$.

Specifically, for $3D \rightarrow 2D$, $A_{3D \rightarrow 2D} \in \mathbb{R}^{N \times N}$ denotes the attention score matrix obtained via the matrix multiplication as follows:

$$A_{3D \rightarrow 2D} = K_{2D} V_{3D}^T, \quad (8)$$

where $K_{2D} = [k_{2D}^1, \dots, k_{2D}^N] \in \mathbb{R}^{N \times F_{2D}}$ and $V_{3D} = [v_{3D}^1, \dots, v_{3D}^N] \in \mathbb{R}^{N \times F_{3D}}$, which can be obtained through Eq. 6, Eq. 7. Moreover, a softmax layer combined with a scaling operation is leveraged to carry out the normalization for attention scores and find the semantically-related regions according to information from another modality $3D$ branch, which can be calculated as follows:

$$R_{3D \rightarrow 2D} = \text{Softmax} \left(\frac{A_{3D \rightarrow 2D}}{\sqrt{F_{2D}}} \right) V_{2D}, \quad (9)$$

where $V_{2D} = [v_{2D}^1, v_{2D}^2, \dots, v_{2D}^N] \in \mathbb{R}^{N \times F_{2D}}$, and $R_{3D \rightarrow 2D} \in \mathbb{R}^{N \times F_{2D}}$ represents the encoded semantic relations from $3D$ to $2D$ features. After that, the $R_{3D \rightarrow 2D}$ is reshaped to the same dimension as the backbone features $f_{2D} \in \mathbb{R}^{F_{2D} \times N}$ and then fused with f_{2D} by an element-wise addition, in order to enhance the semantically similar backbone features.

For $2D \rightarrow 3D$, the $R_{2D \rightarrow 3D} \in \mathbb{R}^{N \times F_{3D}}$ can be easily obtained by performing a symmetrical process described above, which can be written as follows:

$$\begin{aligned} \mathbf{A}_{2D \rightarrow 3D} &= K_{3D} V_{2D}^T, \\ R_{2D \rightarrow 3D} &= \text{Softmax} \left(\frac{\mathbf{A}_{2D \rightarrow 3D}}{\sqrt{F_{3D}}} \right) V_{3D}. \end{aligned} \quad (10)$$

B. Evaluation

Similar to previous 3D point cloud-based Domain Adaptation (DA) methods [16, 9, 29], the performance of the network is evaluated on the test set by leveraging the standard PASCAL VOC Intersection-Over-Union (IoU). The mean IoU (mIoU) is the mean of all IoU values over all classes. In detail, the mIoU can be calculated as follows:

$$\text{mIoU} = \frac{1}{C} \sum_{i=0}^C \frac{TP(i)}{TP(i) + FP(i) + FN(i)}, \quad (11)$$

where C is the overall number of categories, $TP(i)$, $FP(i)$, and $FN(i)$ are values of true positive, false positive, and false negative towards the i -th category, respectively.

C. Module-level Ablation Studies.

Fig. 5 and Fig. 6 vividly depicts the comparison of the four baselines. **Baseline 1** only leverages $2D$ features extracted by the $2D$ backbone. The $2D$ scores obtained by the domain discriminator \mathcal{D} are used to sample the source and target data. **Baseline 2** utilizes the $3D$ features for sampling, where the sampling process will depend on the $3D$ scores from the domain discriminator \mathcal{D} . **Baseline 3** naively averages the $2D$ and $3D$ scores for the sampling strategy. For the first two baselines, since the scores are calculated from a single modality, the sampled data might be distributed in a single modality. For instance, the data sampled by the $2D$ scores will concentrate more on the image information and vice versa. Compared with the above-mentioned baselines, our proposed cross-modal attention-based source-and-target sampling strategy performs an image-to-point and point-to-image feature-level information interaction by a symmetrical cross-branch attention structure. And the cross-modal features are leveraged to train a domain discriminator \mathcal{D} . In this way, the sampled data could take both the $2D$ and $3D$ features into consideration.

D. More Results on 3D ADA Task

In addition to the performance on the ADA task, we further carry out experiments on changing the budget of the target-domain annotation under the Day/Night and A2D2/SemanticKITTI scenarios. As shown in Figs. 7 and 8, consistent with the USA/Singapore setting in the

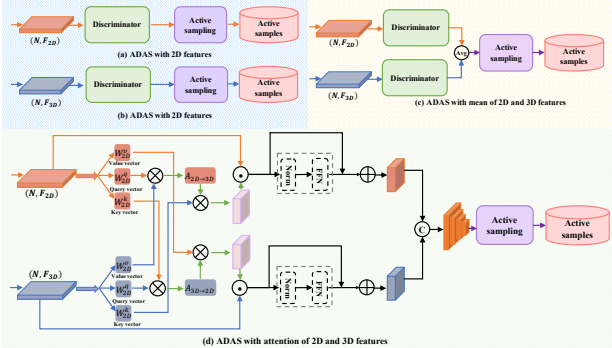


Figure 6. The illustration of various sampling strategies: (a) Baseline 1 means that the key samples are selected only using 2D scores; (b) Baseline 2 means that the key samples are selected only using 3D scores; (c) Baseline 3 means that we sample the keyframes by means of an average across 2D and 3D scores; (d) Ours denotes the sampling scores that are calculated by the cross-attention along the 2D and 3D features.

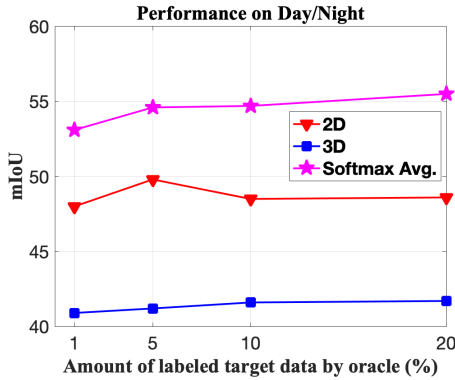


Figure 7. The influence of different target-domain annotation budget \mathcal{B} (20%, 10%, 5%, and 1%) on the ADA task. Here, we take the Day-to-Night scenario as an example.

main text, the UniDA3D also further gradually boosts the target-domain segmentation accuracy. In detail, the model performance in the target domain is improved with the increase of the annotation budget. We also observe that the 5% annotation budget can be regarded as a good trade-off between the annotation cost and the model adaptability.

E. The Visualization of the Selected Samples

In order to comprehensively verify the effectiveness of the cross-modal attention-based source-and-target sampling strategy, the selected samples for both source and target domains are shown in Figs. 9, 10, and 11.

Selected Samples from Day/Night Scenario. As can be seen in Fig. 9, the sampled source data tend to be dark, which is closer to the Night setting in the target domain. And the sampled target data is various, leading to a maximally-informative subset.

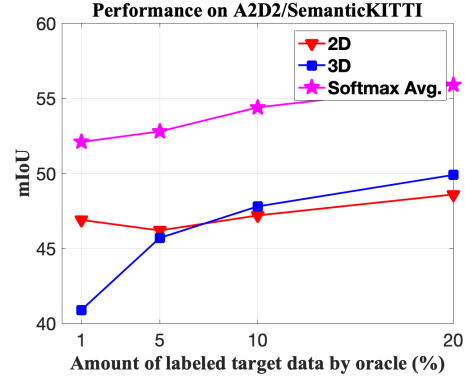


Figure 8. The influence of different target-domain annotation budget \mathcal{B} (20%, 10%, 5%, and 1%) on the ADA task. Here, we take the A2D2-to-SemanticKITTI scenario as an example.

Selected Samples from USA/Singapore Scenario. As shown in Fig 10, the roads in the target domain are relatively narrow, so the source domain data selected by the source-domain sampling strategy are more inclined to the narrow roads in the USA. On the other hand, the target-domain sampling strategy also can select the representative sample.

Selected Samples from A2D2/SemanticKITTI Scenario. As seen in Fig 11, the SemanticKITTI contains various frames that the cars parked along the road. Therefore, our source-domain sampling strategy tends to choose similar frames to the target domain. The tuition is that the selected source data also contains many cars along the streets.

F. More Results on the nuScenes Lidarseg: USA/Singapore.

We also conduct extensive experiments on the nuScenes LiDARSeg [3] to show the superiority of our UniDA3D. Similar to our DA experiments on the other scenarios, we perform our UniDA3D on the USA/Singapore adaptation scenario. The experimental results are shown in Table 5. It can be observed that the baseline model trained on the source domain itself obtains 58.8%, 63.2%, and 68.5% on the 2D, 3D, and softmax average performance, respectively. After the baseline is adapted to the data selected by the source-domain sampling, the segmentation results further increase to 66.6%, 61.0%, and 71.3%, respectively. Besides, the baseline model can be further enhanced by adapting the model to the selected target data, leading to 67.8%, 61.5%, and 72.8% segmentation results. As a result, the baseline model coupled with our UniDA3D is superior to the xMUDA by 1.6% and 1.7% in terms of the 2D and softmax average performance, demonstrating the feasibility and strength of our UniDA3D.

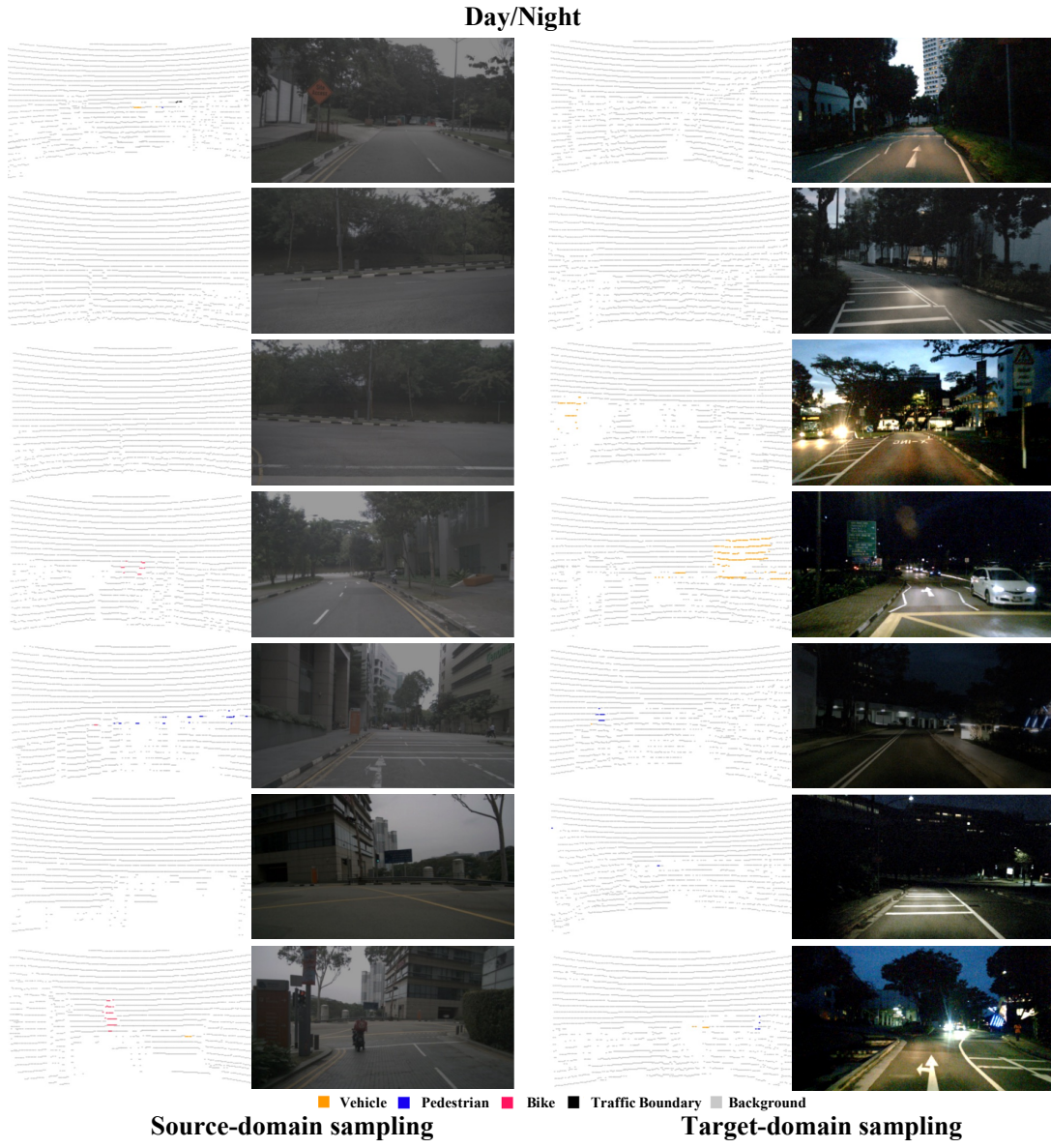


Figure 9. The samples selected by source-domain sampling and target-domain sampling under the Day/Night scenario, where the model tends to select the source-domain data at dark, since the target-domain scenes mainly cover the night scene.

nuSc-LiDARSeg: USA/Singapore	2D	3D	Softmax avg.
Source only	58.8	63.2	68.5
xMUDA	63.1	64.2	67.8
xMUDA + PL	66.2	65.1	70.1
Baseline + Source-domain sampling	66.6	61.0	71.3
Baseline + Source-domain sampling + Target-domain sampling	67.8	61.5	72.8

Table 5. Segmentation results (mIoU) for the UDA setting and ADA setting (5% target-domain annotation budget) under the nuScenes-LiDARSeg USA/Singapore setting.

A2D2 class	Mapped class	SemanticKITTI class	Mapped class
Car 1	car	unlabeled	ignore
Car 2	car	outlier	ignore
Car 3	car	car	car
Car 4	car	bicycle	bike
Bicycle 1	bike	bus	ignore
Bicycle 2	bike	motorcycle	bike
Bicycle 3	bike	on-rails	ignore
Bicycle 4	bike	truck	truck
Pedestrian 1	person	other-vehicle	ignore
Pedestrian 2	person	person	person
Pedestrian 3	person	bicyclist	bike
Truck 1	truck	motorcyclist	bike
Truck 2	truck	road	road
Truck 3	truck	parking	parking
Small vehicles 1	bike	sidewalk	sidewalk
Small vehicles 2	bike	other-ground	ignore
Small vehicles 3	bike	building	building
Traffic signal 1	other-objects	fence	other-objects
Traffic signal 2	other-objects	other-structure	ignore
Traffic signal 3	other-objects	lane-marking	road
Traffic sign 1	other-objects	vegetation	nature
Traffic sign 2	other-objects	trunk	nature
Traffic sign 3	other-objects	terrain	nature
Utility vehicle 1	ignore	pole	other-objects
Utility vehicle 2	ignore	traffic-sign	other-objects
Sidebars	other-objects	other-object	other-objects
Speed bumper	other-objects	moving-car	car
Curbstone	sidewalk	moving-bicyclist	bike
Solid line	road	moving-person	person
Irrelevant signs	other-objects	moving-motorcyclist	bike
Road blocks	other-objects	moving-on-rails	ignore
Tractor	ignore	moving-bus	ignore
Non-driveable street	ignore	moving-truck	truck
Zebra crossing	road	moving-other-vehicle	ignore
Obstacles/trash	other-objects		
Poles	other-objects		
RD restricted area	road		
Animals	other-objects		
Grid structure	other-objects		
Signal corpus	other-objects		
Drivable cobbleston	road		
Electronic traffic	other-objects		
Slow drive area	road		
Nature object	nature		
Parking area	parking		
Sidewalk	sidewalk		
Ego car	car		
Painted driv. instr.	road		
Traffic guide obj.	other-objects		
Dashed line	road		
RD normal street	road		
Sky	ignore		
Buildings	building		
Blurred area	ignore		
Rain dirt	ignore		

Table 6. Class mapping for A2D2/SemanticKITTI scenario.

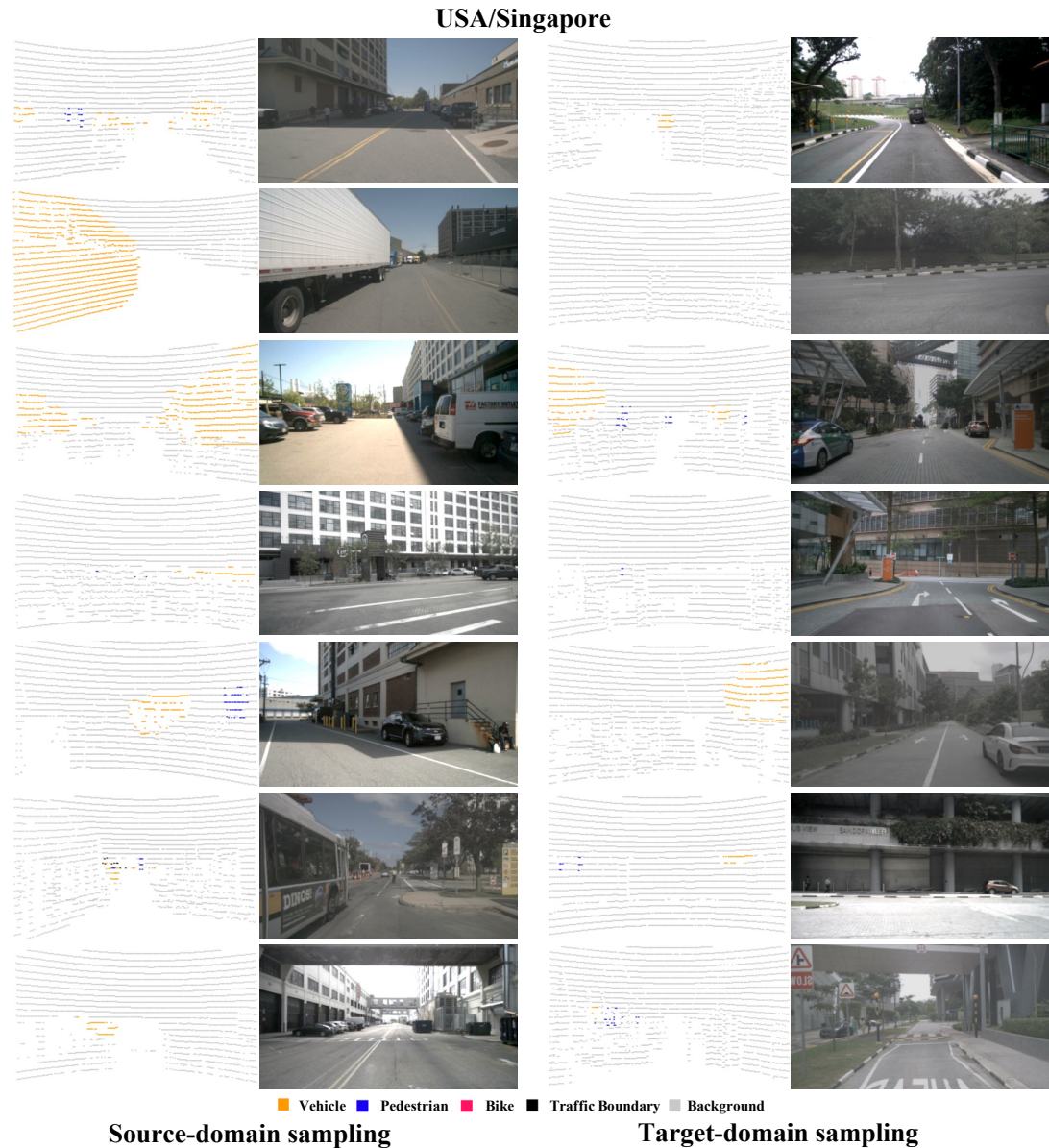


Figure 10. The samples selected by source-domain sampling and target-domain sampling under the USA/Singapore scenario, where the model tends to select the source-domain data collected from the narrow road scene.

A2D2/SemanticKITTI



Figure 11. The samples selected by source-domain sampling and target-domain sampling under the A2D2/SemanticKITTI scenario, where for source domain, various frames that the cars parked along the road are selected by our method.